Electronic Supplementary Material (ESI) for Journal of Materials Chemistry A. This journal is © The Royal Society of Chemistry 2021

A Multifunctional Covalently Linked Graphene-MOF Hybrid as an Effective Chemiresistive Gas Sensor

Kolleboyina Jayaramulu‡*[a,e] Marilyn Esclance DMello‡[b], Kamali Kesavan,[c] Andreas Schneemann,[d] Michal Otyepka,[e] Stepan Kment,[e] Chandrabhas Narayana,[c] Suresh Babu Kalidindi,[f] Rajender S Varma,[e] Radek Zboril,[e] and Roland A. Fischer*[g]

Table of Contents

Table S1: Comparison of Chemiresistive CO_2 sensing values of graphene-based hybrids reported in the literature with our data.

S.N	*Materials*	*Concentration of CO_2*	*Sensing Temperature*	*Resistance of the resistor*	*Sensing conditions*	*Response* %*	*Response time (R_s) (s)*	*Recovery time (R_c) (s)*	*Ref No.*
1	Few-layered Graphene (FLG)	50 ppm	196.8 °C (470 K)	2.236×10^6 Ω	In presence of air	1.8		_	1
2	CVD graphene	1ppm	RT	0.550×10^3 Ω	humidity	>0.0000091	3	_	2
3	Graphene sheet	1 ppm	RT	1.4×10^3 Ω/ RT	44% humidity	0.17	8	_	3
4	Reduced GO-F20	1500 ppm	RT	1.6×10^3 Ω/ RT	34 % RH	71		_	4
5	InkJet Graphene	1 ppm	50 °C	19.7 Ω		0.000235	_	_	5
6	Sb_2O_3 QD/graphene	50 ppm	RT			0.2	16	22	6
7	Y_2O_3/Graphene	35 ppm	_	_	_	1.08	_	_	7
8	Al_2O_3/Graphene	100 ppm	125 °C			10.84	14	22	8

9	PEI/Starch-coated nanotube network FET	100,000 ppm		_	_	20	_	_	9
10	GA@UiO-66-NH_2	500,000 ppm	200 °C	$2.0\times10^4\Omega$	In presence of Ar	8.6	18.5	18.7	This work

_ Values are not reported.

*Calculated Response % based on sensing Figs reported.

RT- Stands for Room Temperature.

RH- Stands for Relative Humidity

ppm- Stands for parts per million.

Ω- Ohms

Table S2: Summary of all pure MOFs studied for chemiresistive gas sensing application.

S.No.	***MOF Sensors***	***Gas/Concentration***	***Sensing Condition***	***Temperature***	***Response %*****	***Response time (s)***	***Recovery time (s)***	***Ref. No.***
1	ZIF-67	Formaldehyde/ 5 ppm	Air	150 °C	1.8	~100	~200	10
2	$[Co(imidazole)_2]_n$	Trimethylamine/ 100 ppm	Air	75 °C	15	1200	1000	11
3	NH_2-UiO-66 (Zr)	SO_2/ 10 ppm	Ar	150 °C	22	26.8	46.1	12
5	$Cu_3(HITP)_2$	Ammonia/ 10 ppm	N_2	RT	2.5	<100	~250	13
6	$Cu_3(HHTP)_2$ Nanofilms	Ammonia/ 100 ppm	Air	RT	129	81.6	546.6	14
7	$Cu_3(HHTP)_2$ Nanorods	NO/ 80 ppm	N_2	RT	1.8	~300	~600	15
8	$Ni_3(HHTP)_2$ Nanorods	H_2S/80 ppm	N_2	RT	4.2	~100	~600	15

9	$Cu_3(HHTP)_2$	Methanol/ 200 ppm	N_2	RT	9	<100	<100	16
10	$Cu_3(HITP)_2$	Ethanol/ 200 ppm	N_2	RT	4	-	-	16
11	$Ni_3(HITP)_2$	Ethanol/ 200 ppm	N_2	RT	4	-	-	16
12	$Cu_3(HIB)_2$	CO_2/ 100 ppm	RH	RT	0.62	420	600	17
13	GA@UiO66-NH_2	CO_2/ 500,000 ppm	Ar	200 °C	8.6	18.5	18.7	This work

**Calculated Response % based on sensing Figs reported.

RT- Stands for Room Temperature.

ppm- Stands for parts per million.

1. Characterization

The synthesized materials were characterized by different techniques. X-ray diffraction (XRD) data of all samples were collected using a X'Pert PRO PANanalytical diffractometer (Bragg-Brentano geometry with automatic divergence slits, position sensitive detector, continuous mode, room temperature, Cu-Kα radiation, Ni filter). The morphology and structure of the materials was characterized through scanning electron microscopy (FESEM-FEI Nova-Nano SEM-600) and transmission electron microscopy (JEOL JEM-3010 with accelerating voltage at 300 kV). X-ray photoelectron spectroscopy (XPS) was performed on a PHI 5000 Versa Probe II scanning XPS microprobe from Physical Electronics, using X-ray radiation from an Al source equipped with a monochromator. Spectra were collected and evaluated with the MultiPak (ULVAC-PHI, Inc.) software. All binding energies were referenced to the C1s peak at 284.8 eV. The Raman spectra of representative samples were collected using a DXR Raman spectrometer (Thermo, USA) with a laser wavelength of 633 nm, laser power on sample of 2 mW, and exposition time of 5 s. Thirty-two spectra were averaged at each spot to obtain one data point. All binding energies were referenced to the C1s peak at 284.8 eV. The porosity of resultant materials was characterized using N_2 physisorption studies. MICROMERITICS ASAP 2020 analyzer was used to carry out the sorption studies at 77 K. All the samples were outgassed at 423 K under high vacuum. The gases (nitrogen, carbon dioxide, and argon) for adsorption studies were obtained from Chemixgases, India, and were 99.99% pure. Raman spectra were recorded using a custom-built Raman spectrometer with a HeNe red laser (632.8 nm) and 1800 lines/mm grating Laser power was 8 mW at the sample. Temperature dependent Raman studies were done using a Linkam THMS 600 heating–cooling stage. Typical accumulation time was 30 s for all the Raman studies. For gas adsorption Raman studies, activated powder GA, **GA@UiO-66-NH$_2$** was mounted on the Linkam stage, and heated to 80 °C and then cooled to room temperature (RT) after which the gases were purged. Temperature was monitored through the temperature controller attached to the Linkam stage. The gas pressure was regulated by the regulator fixed at the inlet and was mostly kept constant around 1 atm. The Raman spectra obtained were smoothened using 5-point FFT, and baseline correction was done to remove the background.

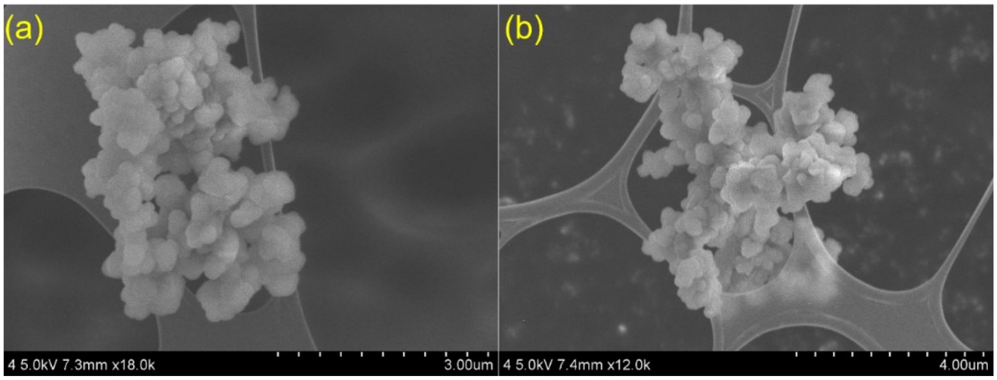

Figure S1. SEM images of pristine Uio-66-NH_2 octahedron nanoparticles with size of 150-200 nm.

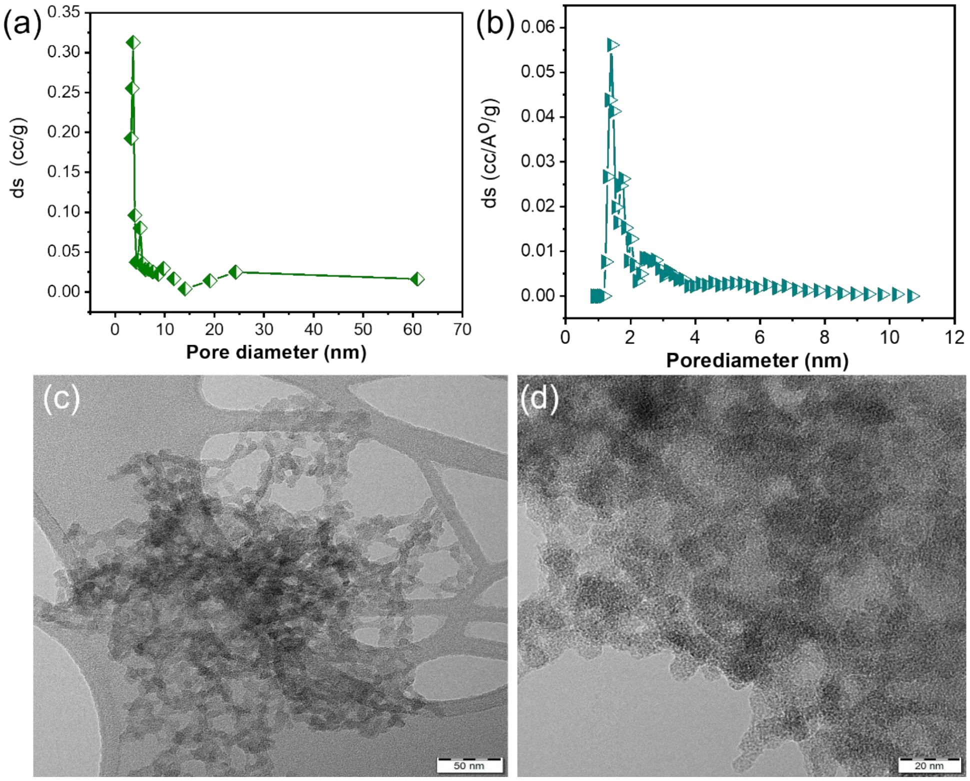

Figure S2. Pore size Distribution **GA@UiO-66-NH_2** shows hierarchical pores (micro-meso) (a) BJH method pore size distribution from Nitrogen adsorption isotherm measured at 77 K (b) NLDFT pore size distribution from Carbon dioxide adsorption isotherm measured at 195 K (c-d) TEM images of hybrids **GA@UiO-66-NH_2** where UiO-66-NH_2 octahedron nanoparticles intercalated with GA layers.

2. Gas sensing measurements

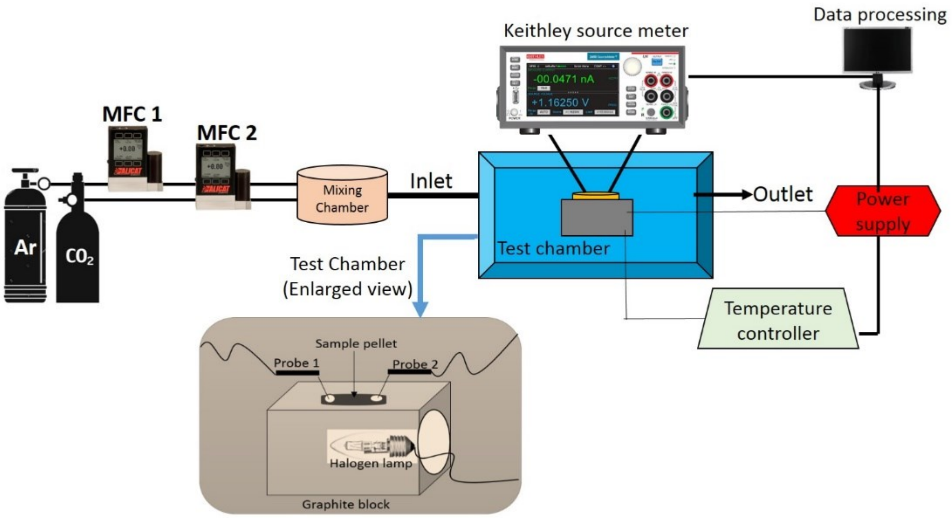

Figure S3. Schematic representation of the custom-built chemiresistive gas sensing device

2.1 Calculation of response percentage of all the sensor materials studied in this work.

The Response of the sensor was defined as

$$\% \text{ Response} = \frac{[R_a - R_g]}{R_a} \times 100$$

Where, R_a= Resistance of the sample in the presence of Argon
R_g= Resistance of the sample in the presence of CO_2

The Response Time (Speed of response) is defined as the time required for a sensor to reach 90 % of total response of the signal such as resistance upon exposure to the target gas.
$T_R = T_2 - T_1$
The Recovery Time is defined as the time required for a sensor to return to 90 % of original baseline signal upon removal of target gas.
Recovery Time = $T_4 - T_3$

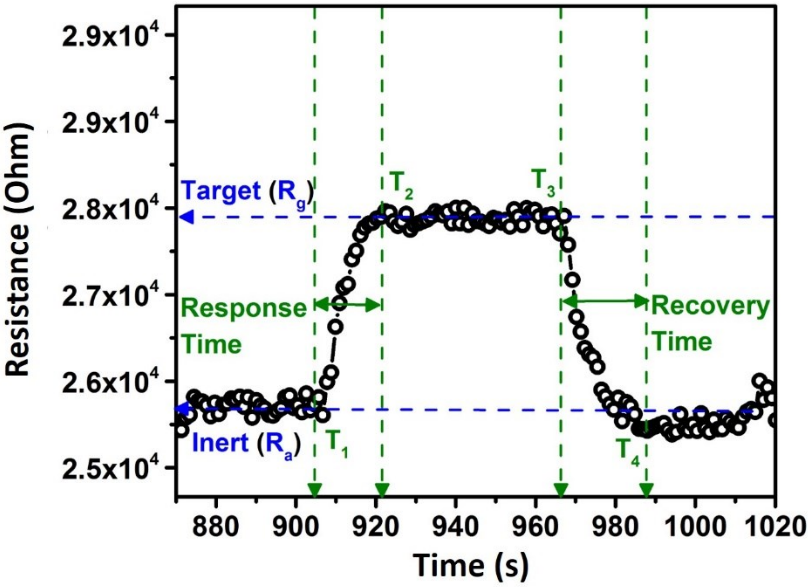

Figure S4. Illustration of the calculation of % response, response time and recovery time studied in this work.

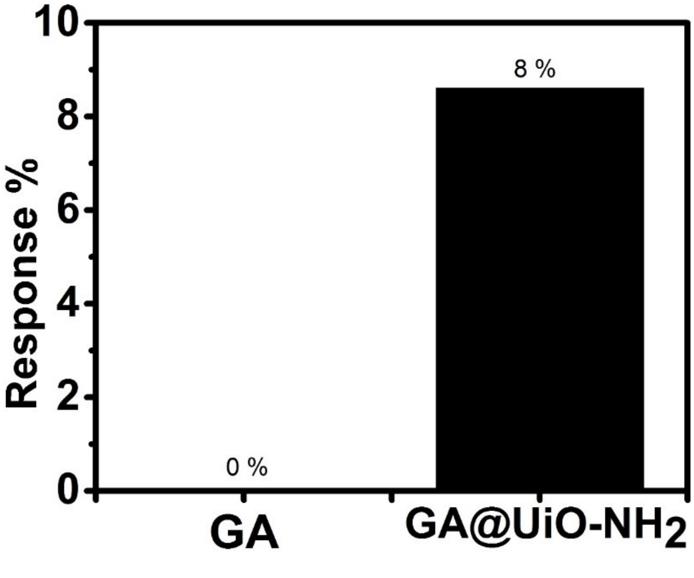

Figure S5. Response of GA and **GA@UiO-66-NH$_2$** towards 50 % CO_2 at 200 °C

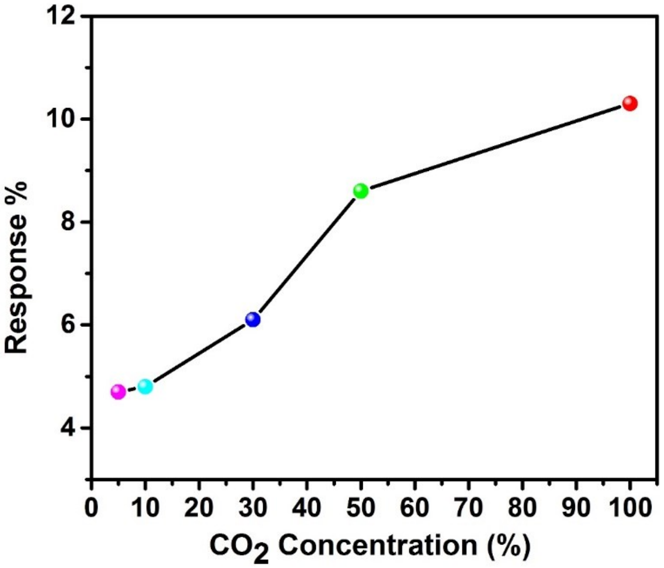

Figure S6. Response of GA@UiO-66-NH$_2$ sensor for a wide range of CO$_2$ concentration.

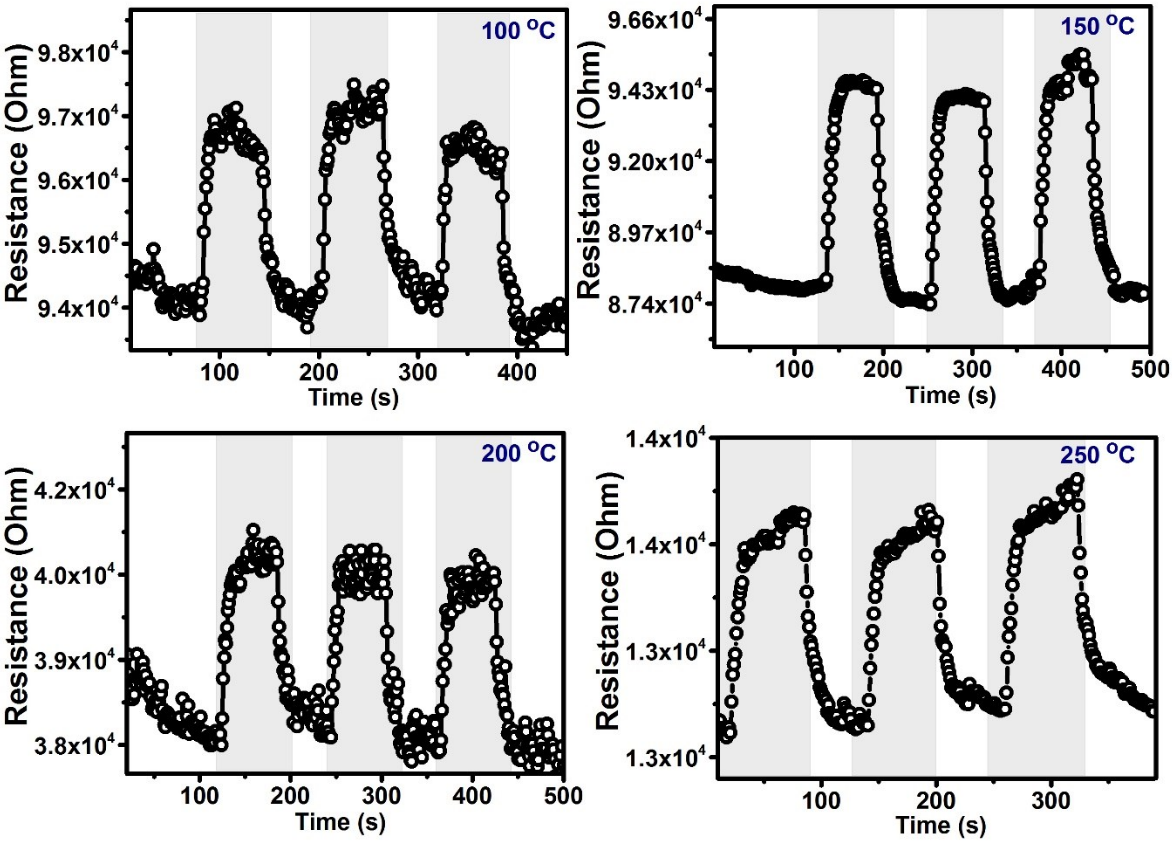

Figure S7. Response-Recovery curves of GA@UiO-66-NH$_2$ to 50 % CO$_2$ balanced with argon at different operating temperatures (100 °C, 150 °C, 200 °C and 250 °C).

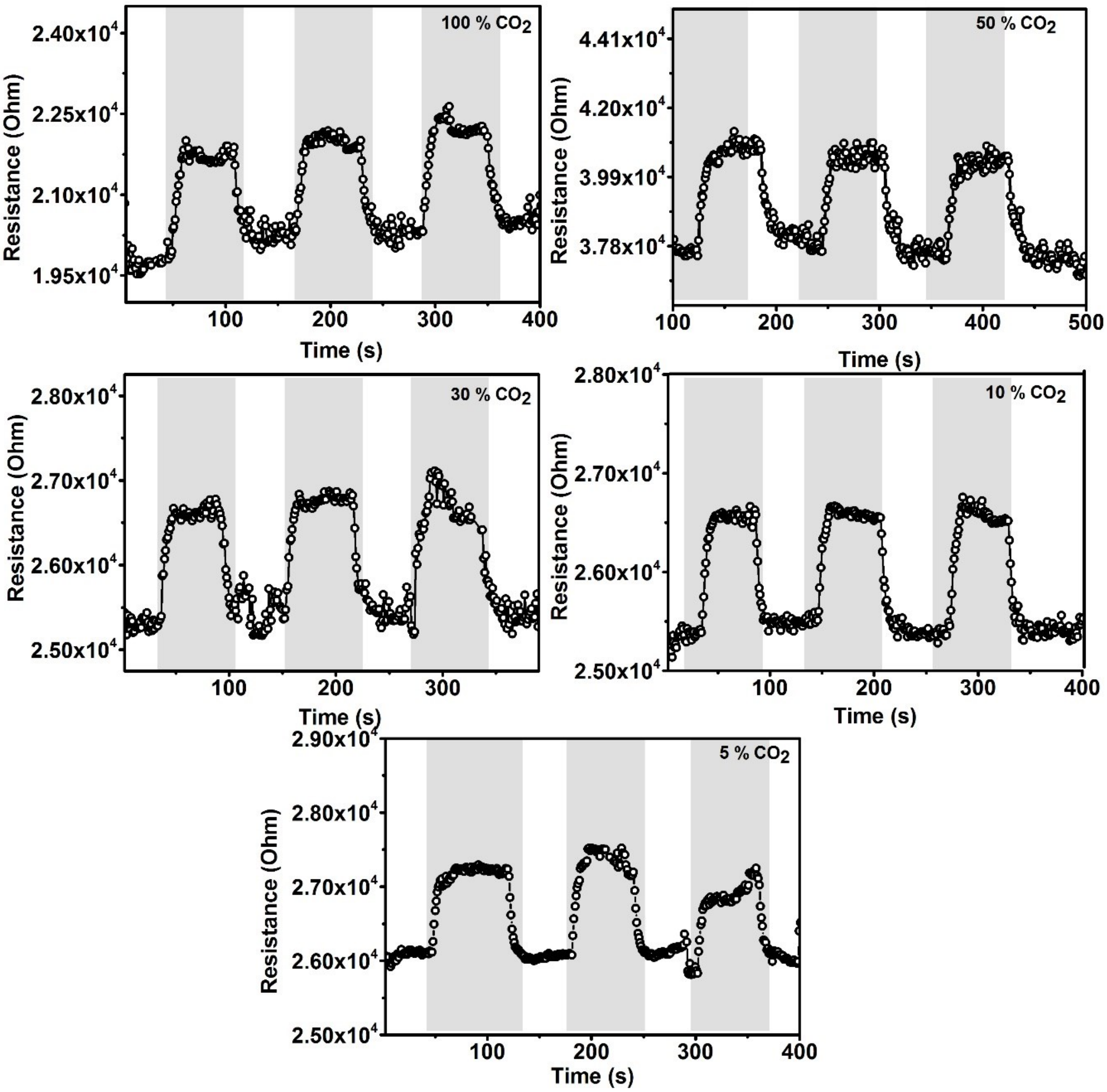

Figure S8. Response-Recovery curves of GA@UiO-66-NH_2 at 200 °C for different quantity of CO_2 (100 %, 50 %, 30 %, 10 % and 5 % CO_2 balanced with argon).

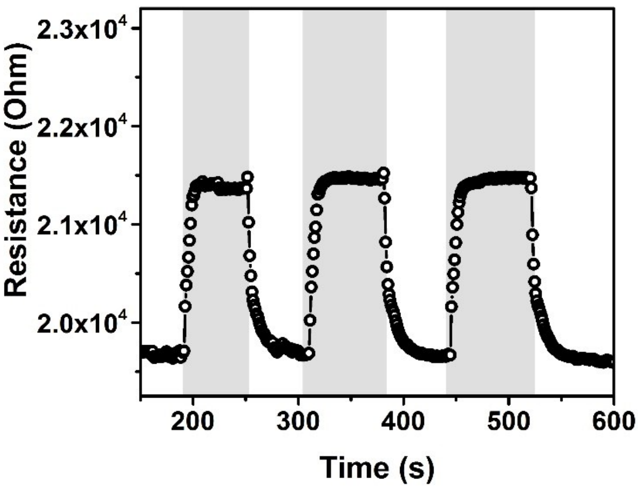

Figure S9: Gas sensing performance of GA@UiO-66-NH_2 in presence of synthetic air to 50 % CO_2 concentration at an operating temperature of 200 °C.

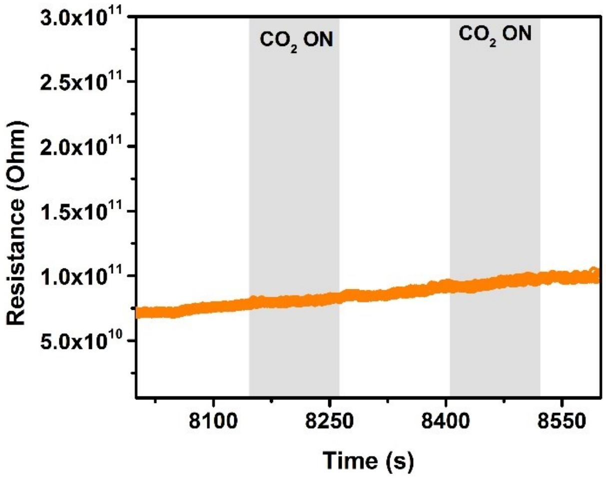

Figure S10: Gas sensing performance of pristine UiO-66 MOF to 50 % CO_2 concentration at an operating temperature of 200 °C.

3. Raman Spectroscopy

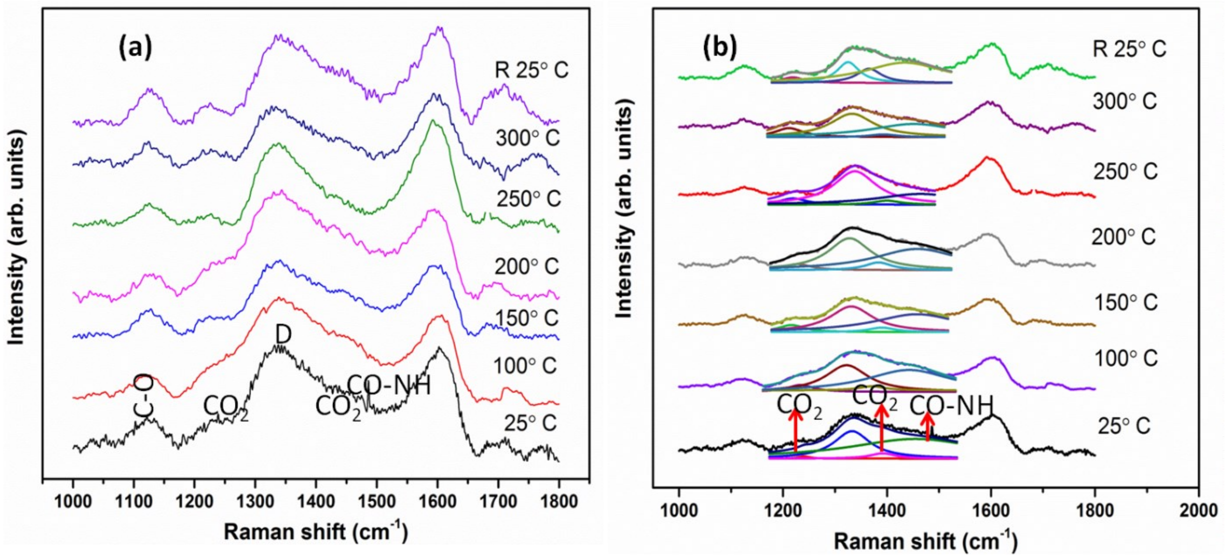

Figure S11. Raman spectra of **GA@UiO66-NH$_2$** in CO$_2$ atmosphere at different temperatures and R denotes reverse cycle and (b) shows the fitted Raman spectra clearly showing CO$_2$ and amide CO-NH linkage.

Discussion: When performing nonlinear curve fitting, an iterative procedure is employed that minimizes the reduced chi-square value to obtain the optimal parameter values. Although this is the quantity that is minimized in the iteration process, this quantity is typically not a good measure to determine the goodness of fit. For example, if the y data is multiplied by a scaling factor, the reduced chi-square will be scaled as well. A better measure would be the r-square value, which is also known as coefficient of determination. The closer the fit is to the data points, the closer r-square will be to the value of 1. A larger value of r-square does not necessarily mean a better fit because the degrees of freedom can also affect the value. Thus, if more parameters are introduced, the r-square value will rise, but this does not imply a better fit. The **adjusted r-square** value accounts for the degrees of freedom and this could be a better measure of the goodness of fit. In the current study, Raman spectra have been fitted using Origin Pro 8.5.1 software. For all the fits, the adjusted r-square value has been considered as a measure of goodness of fit. The below figures figure S12 are enlarged view of figure S11.

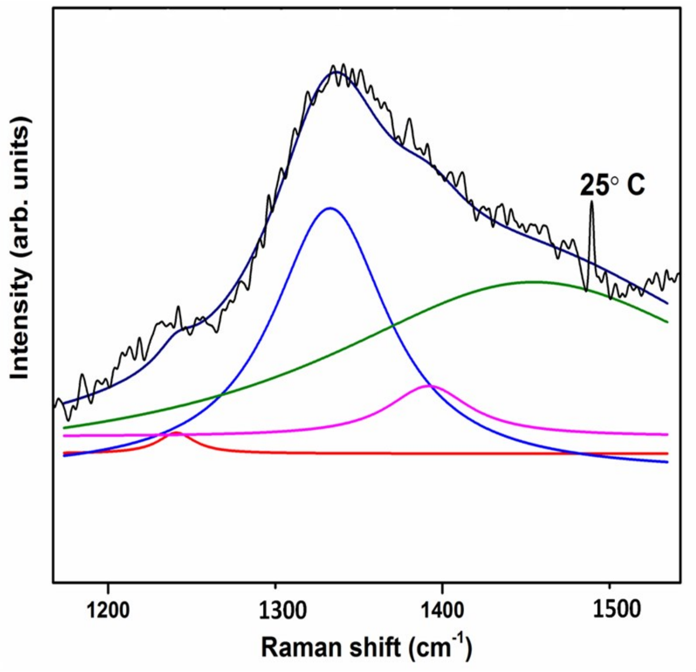

Figure S12. Raman spectrum of **GA@UiO66-NH$_2$** in CO$_2$ atmosphere collected at 25 °C. The spectrum is fitted using Lorentz function. **Adj. R-Square=0.98797**

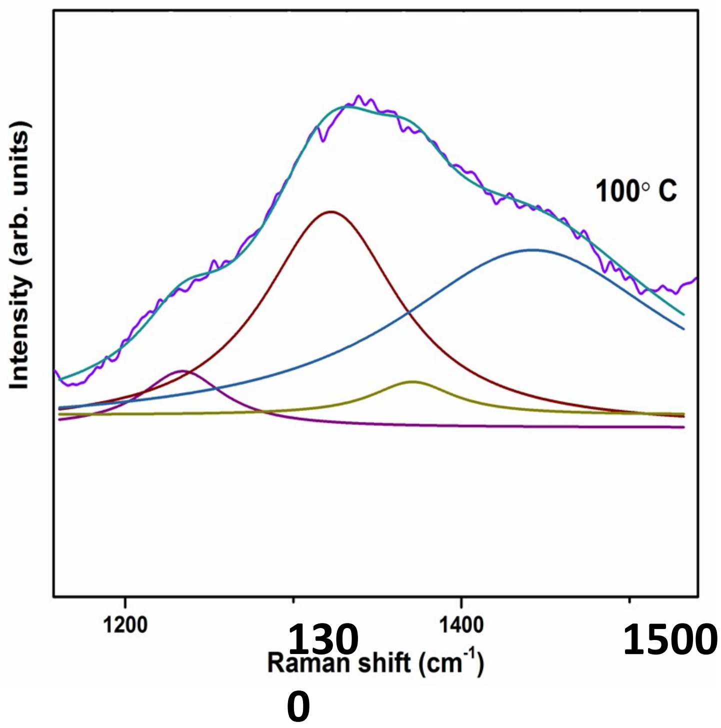

Figure S13. Raman spectrum of **GA@UiO66-NH$_2$** in CO$_2$ atmosphere at 100 °C from 1160-1575 cm^{-1} range. The spectrum is fitted using a Lorentz function. **Adj. R-Square=0.98837**

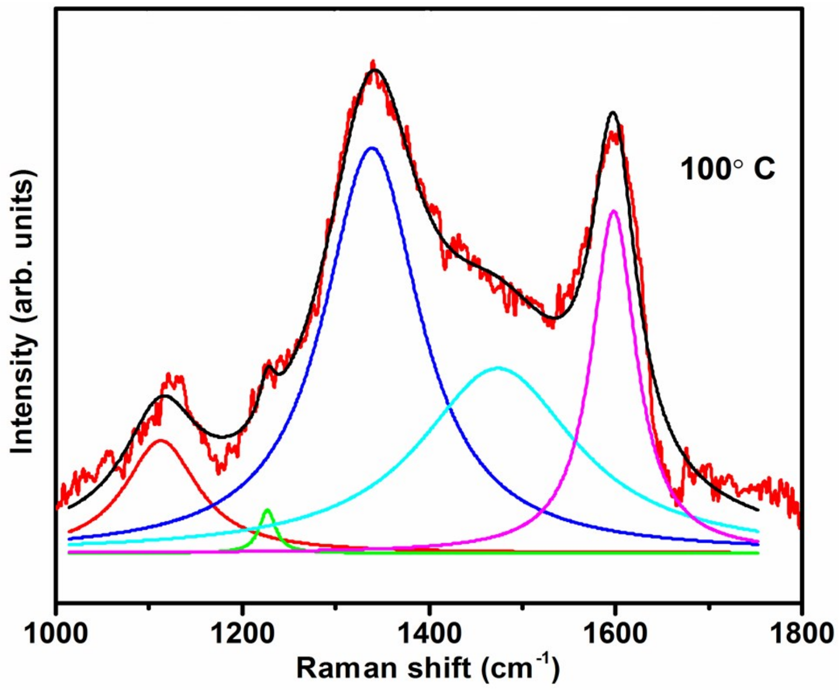

Figure S14. Raman spectrum of **GA@UiO66-NH$_2$** in CO$_2$ atmosphere at 100 °C from 1000-1800 cm^{-1}. Fit were obtained using a Lorentz function. Adj. R-Square value = 0.97809.

Discussion: Fitting in the range from 1000-1800 cm^{-1}, we only obtained an Adj. R-Square value of 0.97809 which is comparatively low compared to the above shown partitioned fitted spectrum at 100 °C. The observed broad shoulder at 1226 cm^{-1}corresponding to the Fermi Resonant CO$_2$ peak shows a less sharp intensity in the fitted spectrum. We could not fit other less intense Fermi Resonant CO$_2$ peak at 1376 cm^{-1}. Hence, we opted for the above partitioned fitting which could fit all the peaks well with reasonable goodness of fit

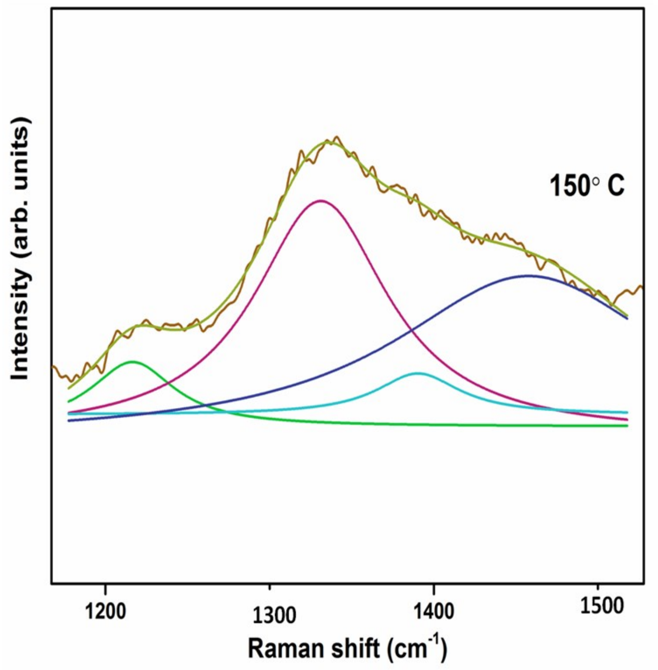

Figure S15. Raman spectrum of **GA@UiO66-NH$_2$** in CO$_2$ atmosphere at 150° °C from 1160-1575 cm^{-1}. The spectrum is fitted using a Lorentz function. **Adj. R-Square=0.98869**

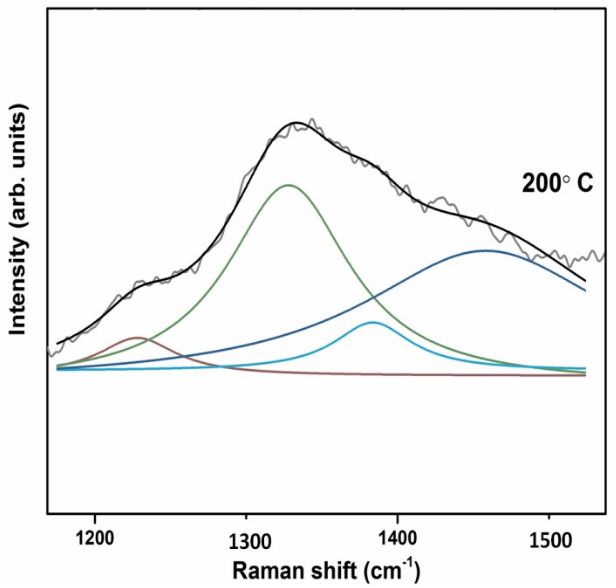

Figure S16. Raman spectrum of **GA@UiO66-NH$_2$** in CO$_2$ atmosphere at 200°C from 1160-1575 cm^{-1}. The spectrum is fitted using a Lorentz function. **Adj. R-Square=0.98859.**

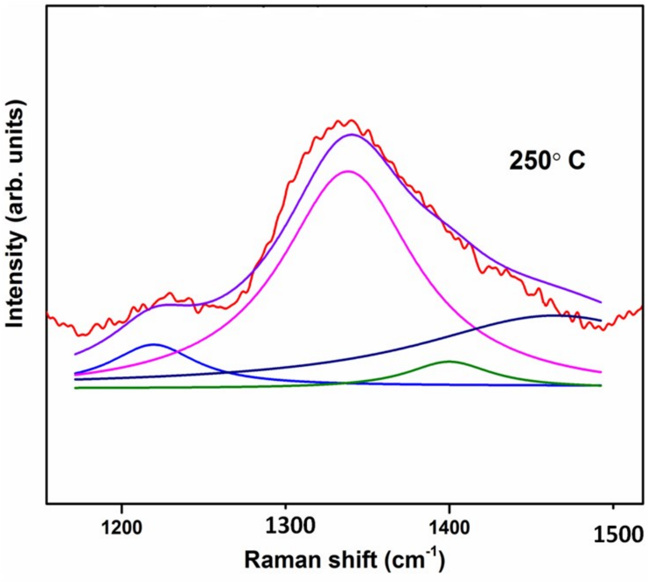

Figure S17. Raman spectrum of **GA@UiO66-NH$_2$** in CO$_2$ atmosphere at 250 °C from 1160-1575 cm^{-1} The spectrum is fitted using Lorentz function. **Adj. R-Square=0.98602**

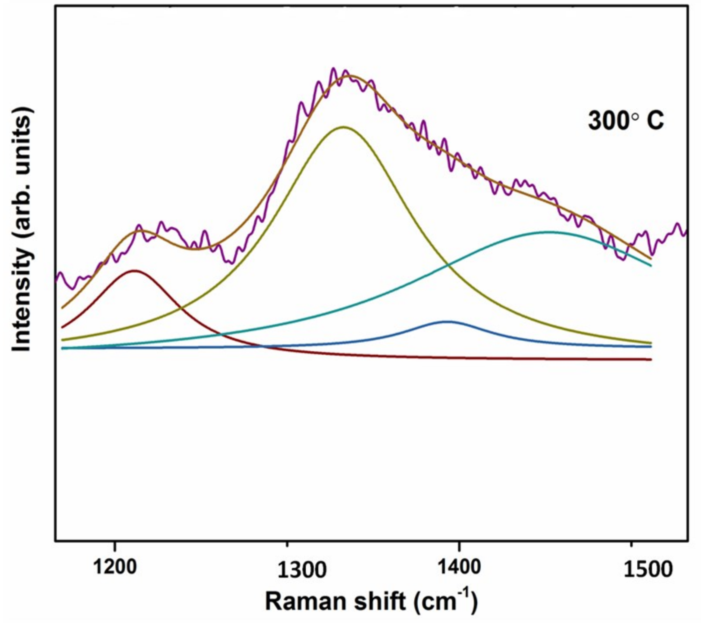

Figure S18. Raman spectra of **GA@UiO66-NH$_2$** in CO$_2$ atmosphere at 300°C from 1160-1575 cm^{-1}. The spectrum is fitted using a Lorentz function. **Adj. R-Square=0.98829**

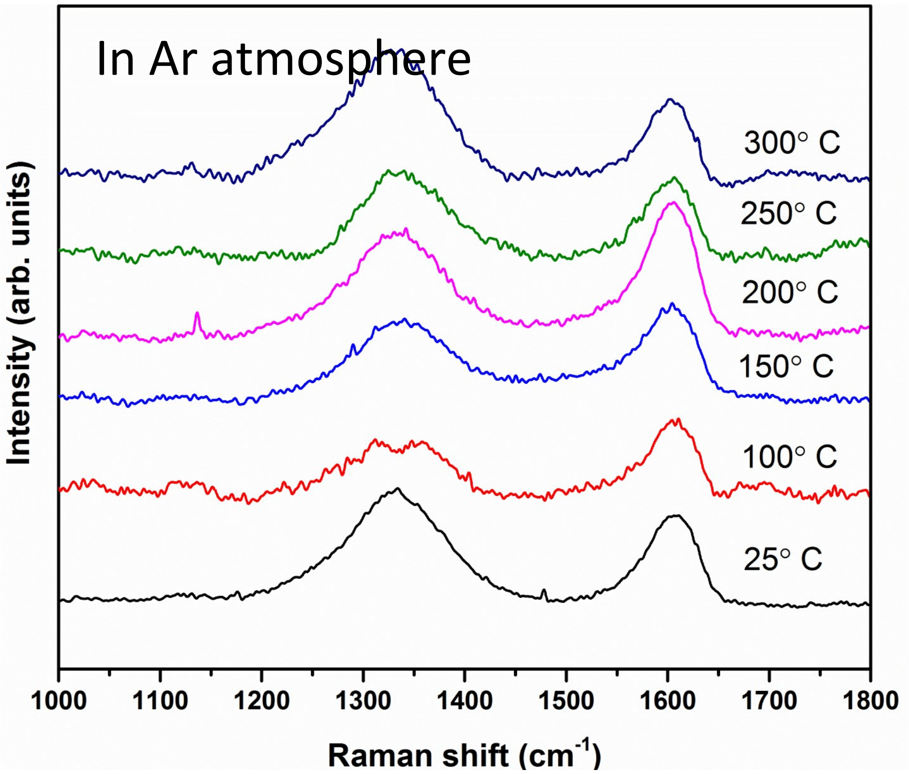

Figure S19. Raman spectra of **GA@UiO-66-NH$_2$** in Ar atmosphere at different temperatures.

4. References

1. Nemade, K. R. &Waghuley, S. A, Chemiresistive gas sensing by few-layered graphene. *J. Electron. Mater*. 42, 2857-2866 (2013).
2. Smith, A.D. et al., Graphene-based CO$_2$ sensing and its cross-sensitivity with humidity. *RSC Adv.* 7, 22329-22339 (2017).
3. Yoon, H.J. et al., Carbon dioxide gas sensor using a graphene sheet. *Sens. Actuator B-Chem.* 157, 310-313 (2011).
4. Hafiz, S.M. et al., A practical carbon dioxide gas sensor using room-temperature hydrogen plasma reduced graphene oxide. *Sens. Actuator B-Chem.* 193, 692-700 (2014).
5. Andò, B. et al., An inkjet printed CO$_2$ gas sensor. *Procedia eng.* 120, 628-631 (2015).
6. Nemade, K. R. &Waghuley, S. A, Role of defects concentration on optical and carbon dioxide gas sensing properties of Sb$_2$O$_3$/graphene composites. *Opt. Mater*. 36, 712-716 (2014).
7. Nemade, K. R. &Waghuley, S. A, Carbon dioxide gas sensing application of graphene/Y$_2$O$_3$ quantum dots composite. *Int. J. Mod. Phys. A*. 22, 380-384 (2013).
8. Nemade, K. R. &Waghuley, S. A, Highly responsive carbon dioxide sensing by graphene/Al$_2$O$_3$ quantum dots composites at low operable temperature. *Indian J. Phys*. 88, 577-583 (2014).

9. Star, A. et al., Nanoelectronic carbon dioxide sensors. *Adv. Mater.*16, 2049-2052 (2004).
10. Chen, E.X., Yang, H. & Zhang, J, Zeolitic imidazolate framework as formaldehyde gas sensor. *Inorg. Chem.,* 53, 5411-5413 (2014).
11. Chen, E.X. et al., Highly selective and sensitive trimethylamine gas sensor based on cobalt imidazolate framework material. *ACS Appl. Mater. Interfaces,* 6, 22871-22875 (2014).
12. DMello, M.E. et al., An amine functionalized zirconium metal–organic framework as an effective chemiresistive sensor for acidic gases. *Chem. Commun*. 55, 349-352 (2019).
13. Campbell, M.G. et al., Cu_3(hexaiminotriphenylene)$_2$: an electrically conductive 2D metal–organic framework for chemiresistive sensing. *Angew. Chem.* 54, 4349-4352 (2015).
14. Yao, M.S. et al., Layer-by-Layer Assembled Conductive Metal–Organic Framework Nanofilms for Room-Temperature Chemiresistive Sensing. *Angew. Chem.* 56, 16510-16514 (2017).
15. Smith, M.K. et al., Direct self-assembly of conductive nanorods of metal–organic frameworks into chemiresistive devices on shrinkable polymer films. *Chem. Mater.* 28, 5264-5268 (2016).
16. Campbell, M.G. et al., Chemiresistive sensor arrays from conductive 2D metal–organic frameworks. *J. Am. Chem. Soc.*, 137, 13780-13783 (2015).
17. I. Stassen, J. Dou, C. Hendon, M. Dincă, Chemiresistive Sensing of Ambient CO2 by an Autogenously Hydrated Cu3(hexaiminobenzene)2 Framework *ACS Cent. Sci.* 2019, 5, 8, 1425-1431.